Nanoscale and Microscale Thermophysical Engineering, 13: 184–201, 2009

ISSN: 1556-7265 print / 1556-7273 online
DOI: 10.1080/15567260903077751

MEASUREMENT OF HEAT TRANSFER DURING DROP-WISE CONDENSATION OF WATER ON POLYETHYLENE

Gagan Deep Bansal, Sameer Khandekar, and K. Muralidhar
Department of Mechanical Engineering, Indian Institute of Technology Kanpur, Kanpur (UP) India

Heat transfer coefficients associated with drop-wise condensation are quite large. Because the ensuing driving temperature difference is small, experimental determination of heat transfer coefficient is a challenge. The statistical nature of droplet distribution in the ensemble contributes to the intricacy of analysis and interpretation. Against this background, the spatial distribution of temperature during drop-wise condensation over a polyethylene substrate was measured using liquid crystal thermography (LCT) simultaneously with actual visualization of the condensation process by videography. Experiments were conducted in such a way that pendant drops form on the underside of the liquid crystal sheet. Temperature variation at the base of the droplets, as small as 0.4 mm, were satisfactorily resolved. The signature of the drop shape was visible in the LCT images. The drop size distribution on the substrate was simultaneously visualized. Static contact angles of water on polyethylene are measured and drop shapes were estimated via a mathematical model for comparison. Using a one-dimensional heat transfer approximation, heat flux profiles through individual droplets were obtained. The temperature profiles from LCT combined with drop sizes from direct visualization provide sufficient data for understanding the heat transfer mechanism during drop-wise condensation. Results show that the measured heat flux as a function of drop diameter matches published data for large drop sizes but fails for small drops where the thermal resistance of the LCT sheet is a limiting factor. To a first approximation, the present work shows that drop size can be correlated to the local heat flux. Hence, the average heat flux over a surface can be obtained entirely from the drop size distribution.

KEY WORDS: drop-wise condensation, heat transfer, drop size distribution, liquid crystal thermography

INTRODUCTION

When compared to heat transfer through liquid films, significantly higher heat transfer coefficients are achievable in drop-wise condensation. Substantial saving in material and energy can result if the presupposition of film-wise condensation, normally the basis for condenser design calculations, could be changed to drop-wise

Manuscript accepted 1 May 2009.
The project was funded by the Board of Research in Nuclear Sciences (BRNS), Department of Atomic Energy, Government of India, under project #ME/BRNS/20050106. Technical support from Mr. C. S. Goswami is appreciated.
Address correspondence to Sameer Khandekar, Department of Mechanical Engineering, Indian Institute of Technology Kanpur, Grand Trunk Road, Kanpur (UP) 208016, India. E-mail: samkhan@iitk.ac.in

NOMENCLATURE

A	area, m^2
D	diameter, m
g	acceleration due to gravity, m/s^2
H, S, I	hue, saturation, intensity scale
h	heat transfer coefficient, W/m^2-K
h_{fg}	latent heat, J/kg
K_1	constant
k	thermal conductivity, W/m-K
M	molecular weight, kg/kmol
n	number density, m^{-2}
P	pressure, N/m^2
$\dot{Q}$	heat transfer rate, W
q''	heat flux, W/m^2
$\tilde{R}$	gas constant, J/K-mol
R, G, B	red, green, blue scale
T	temperature, K
$\bar{T}$	average temperature, K
t	thickness, m

Greek Symbols

λ	wavelength of light, m
ρ	density, kg/m^3
$\hat{\sigma}$	accommodation coefficient
σ	surface tension, N/m
υ	specific volume, m^3/kg

Subscripts

avg	average value
exp	experimental
liq	liquid
max	maximum
min	minimum
pix	digitized pixel
sat	saturation
sub	substrate
total	total value
vap	vapor
w	cooling water

condensation. In an engineering device, the condition of drop-wise condensation is realized by appropriately texturing or suitably modifying the surfaces exposed to vapor [1–3]. There is a renewed interest in fully understanding the drop-wise mode of condensation due to the possibility of engineering surfaces; namely, by physical and chemical texturing as well as surface modification [4–6]. Complementary interest for miniaturization and compactness of heat transfer equipment [7] is also to be addressed.

In spite of sustained research in the past decades, many issues related to heat transfer during drop-wise condensation remain unresolved [1, 8]. This is mainly because small changes in the surface morphology on a micro/nanoscale and, hence, surface energy, lead to changes in the droplet distribution, affecting the ensuing thermohydrodynamics. In addition, the overall mechanism of formation of a droplet on an engineering surface involves varied length scales, from atomistic orders at early phases of nucleation on one hand to scales affected by the body force distribution vis-à-vis the surface tension forces on the other [9]. These changes can only be understood when a multiscale modeling approach is adopted [10]. In addition, changes in contact angles and the hysteresis phenomenon of the contact line remain as heuristic parameters in the predictive models. Frequently, sessile or pendant droplets on substrates are modeled as hemispheres completely neglecting the dynamic contact angles that appear in real-time operation [11]. Very high heat transfer rates (and therefore very low temperature differential) coupled with the above factors also hinder generation of repeatable experimental data. Thus, experiments that concern heat transfer during drop-wise condensation are quite complex [1–3, 7, 8].

A common assumption in heat transfer analysis and the interpretation of experimental data is the isothermal nature of the substrate on which condensation is taking place. Quite often, the temperature gradient in the normal direction, recorded in the bulk substrate by suitably located thermocouples, is extrapolated to determine the

average temperature of the substrate [11, 12]. Subsequently, average condensation heat transfer coefficients are determined. However, the inherent droplet size distribution on the substrate, which in turn is time dependent, results in surface temperature fluctuations during the sequence of condensation, coalescence, and removal of the drops. Such a variation of temperature/heat flux at the base of each condensing drop is obvious when we consider a mechanistic model [13, 14]. Neglecting these details will lead to an error in determining the real heat transfer coefficient.

Although the inherent time dependence of heat transfer in drop-wise condensation has been acknowledged in the literature, spatiotemporal determination of temperature fluctuations is not straightforward. Need for such data generation is essential to relate the droplet ensemble hydrodynamics to the consequent integrated thermal-hydrodynamic process performance. Conventional thermometry (e.g., with thermocouples) cannot provide spatial information of temperature distribution. Moreover, for measurements on mini/microscales (as in the case of individual condensing droplets), spatial constraints and sensor intrusion thwarts the acquisition of primary information at the desired level of accuracy. For this reason, liquid crystal thermography (LCT) has been used in the present study. The spatiotemporal variation of temperature (and therefore the heat flux passing through the surface in the normal direction) can be obtained from LCT. The technique and methodology allows the determination of the thermal behavior on the scale of a single condensate drop.

In the present work, the fluid considered is pure deionized water condensing under controlled conditions on the underside of a polyethylene substrate. Study of stand-alone polymer substrates as well as polymer-coated metal substrates subjected to drop-wise condensation has immense practical engineering applications not only for dedicated heat transfer applications but also for other engineering systems ranging from compact polymer heat exchangers, contact lenses, thermal enclosures for horticulture applications, and dew formation on polymer food packages, to name a few [15–18]. Videography and high-spatial-resolution LCT are simultaneously employed to derive information on the condensing droplets. A specially designed experimental setup enables in situ measurements of condensation over a suitably textured surface. Results obtained are compared with the classical one-dimensional heat transfer formulation of drop-wise condensation [12–14].

EXPERIMENTAL SETUP

The experimental apparatus has been designed to study drop-wise condensation under controlled conditions on the underside of a substrate. A unique feature of the designed apparatus is that it permits simultaneous visualization of the condensing droplets and temperature measurement using liquid crystal thermography, both as a function of time. As seen in Figure 1, the setup primarily consists of a main cylindrical polycarbonate vacuum chamber of inner diameter 180 mm and length 110 mm. It is closed from the two ends by specially designed flanges. The lower brass flange is fitted with a $\lambda/4$ optical viewing window (View A). The wavelength referred to in this discussion is that of visible light. In addition, it also has an annular space around this viewing window wherein the working fluid inventory is stored. A circular, 1.5-mm-thick mica strip heater (OD = 70 mm, ID = 40 mm) is attached outside this annular space to give the necessary heat input, as detailed in the figure. The upper end of the main vacuum chamber is sealed with a polycarbonate flange fitted with a transparent

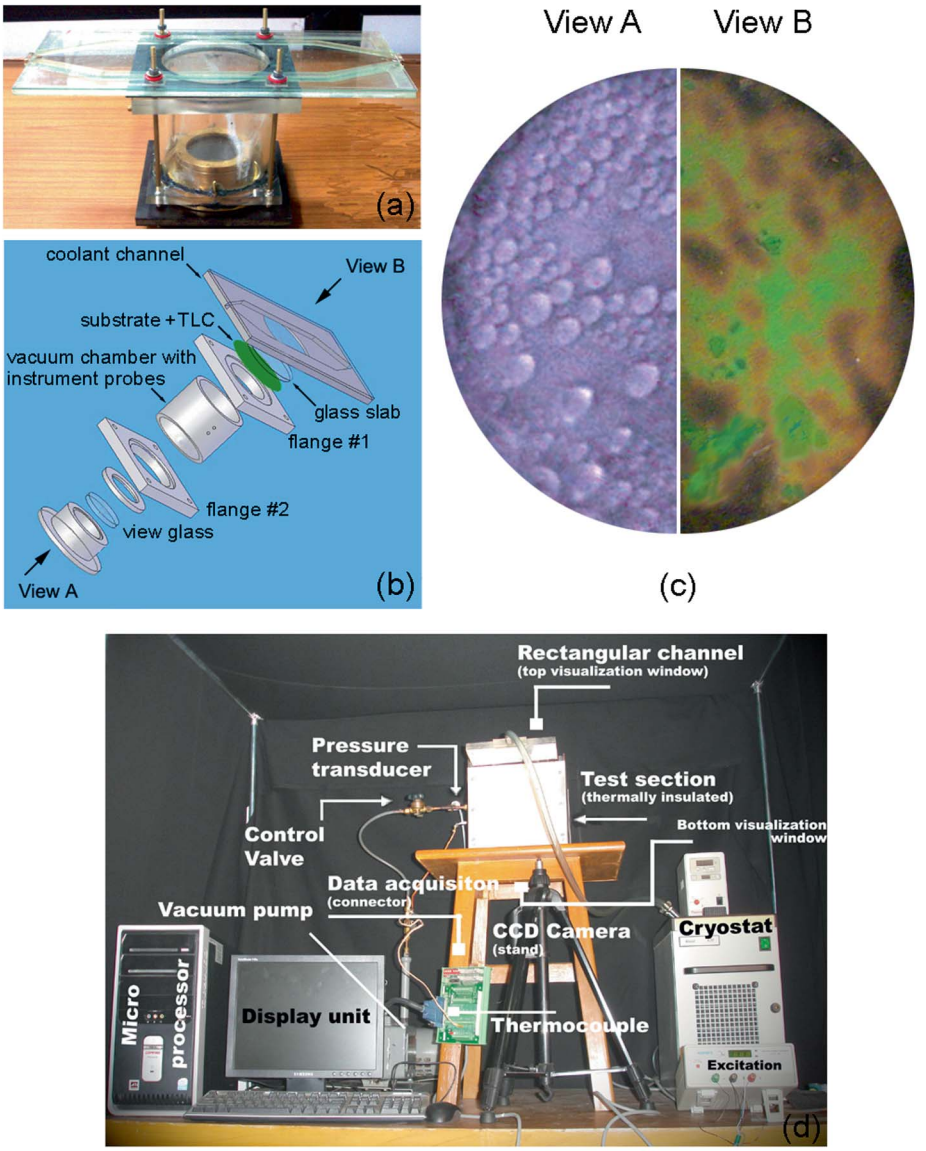

Figure 1. Details of the experimental setup to study drop-wise condensation on the underside of a substrate. (a) Photograph shows the details of the main condensing chamber; (b) exploded view of the condensing chamber showing all the components. (c) Camera View A (refer (b)) from the bottom gives the actual photograph of the condensing droplets, whereas Camera View B provides the RGB image of the TLC. (d) Details of the peripheral systems of the setup. (Figure appears in color online).

$\lambda/4$ optical glass disk of 100 mm diameter and 8.0 mm thickness. Outside the glass disk, a coolant passage of rectangular section (200 mm $\times$ 6 mm) is provided so that one face of the glass disk can be subjected to constant temperature boundary conditions by varying the temperature of the flowing coolant. The walls of the coolant passages are

also made of transparent polycarbonate Makrolon® material. The whole assembly chamber is made vacuum tight ($<10^{-6}$ mbar) by doing the assembly with O-rings.

Connections for evacuation, pressure transducer, and temperature sensor are provided on the main chamber wall. Condensing vapor temperature is measured with calibrated K-type thermocouples (National Instruments®) of accuracy ± 0.05°C, after calibration, which is placed centrally in the chamber at a distance of 25 mm from the side wall. The condensing chamber pressure is measured by an absolute pressure transducer (M/s Honeywell®, accuracy 0.1%FS, NIST traceable calibration, range 0–1.2 bar). Online data acquisition with 16-bit PCI-4351 card (National Instruments®) connected to a PC has been carried out.

A color CCD camera (Basler® A202KC resolution: 1024×1024) is used to capture the LCT images (View B) and a Sony digital camera with CCD sensor is used for capturing the actual optical video images of the condensing surface (View A). A diffuse white light source with controllable output is used for illumination.

EXPERIMENTAL METHODOLOGY

Calibration of TLCs

Liquid crystals supplied by M/s Hallcrest®, in microencapsulated form, displaying the full RGB color spectrum are used in the present study (the nominal identification of the crystals by the supplier is 'R40C5W'; i.e., Red Start at 40°C with a bandwidth of 5°C, bandwidth being defined as the blue start temperature minus the red start temperature [19]). These crystals respond to changes in temperature by changing their color. They have chiral (twisted) molecular structures and are optically active mixtures of organic chemicals turning from colorless (black against a black background) to red at a given temperature (called the *event temperature*) and, as the temperature is increased, passing through the other colors of the visible spectrum in sequence (orange, yellow, green, blue, violet) before turning colorless (or black) again at a higher temperature, called the *clearing temperature*. The color changes are reversible; on cooling, this color change sequence is reversed. Thus, the local spatial temperature distribution can be captured by a digitizer (e.g., a CCD camera with a frame grabber card) and suitably quantified in 8/16-bit pixel-specific information. This pixelized response, corresponding to the local temperature, is usually available in the form of the three primary colors: red, green, and blue (RGB). To relate these to temperature, the color response needs to be reduced to a single value. This step is accomplished by converting the pixel-level RGB values to the HSI (hue, saturation, and intensity) and choosing the hue parameter to scale with temperature. The important reason for the choice of hue as the discriminating parameter is the fact that it is practically independent of light intensity or illumination [20].

A polyethylene sheet (70 μm thick) coated with the encapsulated liquid crystals is attached on the lower surface of the top optical window. Drop-wise condensation takes place directly on the polyethylene sheet. Before commencement of the drop-wise condensation experiments, in situ calibration was carefully conducted under controlled conditions. It is important to perform the calibration in situ so that identical lighting conditions exist during calibration and the main experiments. To allow for minor changes in surface quality and the light source, calibration is repeated after two

full runs of the experiment. Calibration of the LCT sheet was performed as follows. Without the evaporator heater power, water was circulated using a high end kelvimat (HAAKE® DC10K20; accuracy ± 0.1°C) at controlled temperature steps between the operational bandwidth of the LCT sheet. A precalibrated Pt-100 thermocouple (accuracy ± 0.05°C) placed on the substrate was used as the reference. A region of interest (ROI) was selected for constructing the calibration curve. Although the minimum size for a given ROI is a single pixel, a size greater than one pixel was utilized to statistically account for noisy pixels. Considering scatter in the hue values, the nominal hue value was based on the median of the hue distribution. A fifth-order polynomial was used to fit the calibration data relating hue and temperature as measured by the thermocouple [20, 21]. Figure 2 shows a sample calibration curve drawn between hue and the operating substrate temperature; the corresponding recorded RGB images of the ROI by the color CCD camera (Basler®-A202KC) are also shown. Subsequent experiments have been carried out under identical conditions of illumination with identical laboratory environmental conditions. Following the procedure given by Hay and Hollingsworth [22], the overall accuracy of the measurement process is estimated to be 0.42°C. This is about 6% of the useful range of the LCT and compares well with other reported experimental data on capsulated LCT studies [21, 23]. It includes uncertainty in the primary thermocouple sensors, sensitivity of hue calculation from RGB values, and standard error estimate of curve fitting.

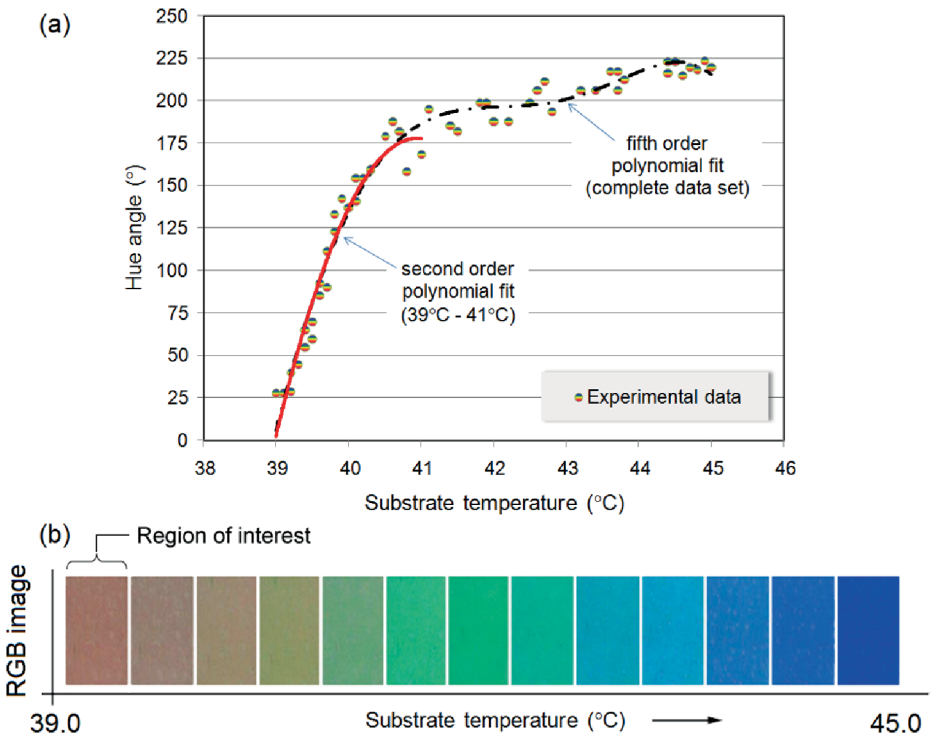

Figure 2. (a) Typical calibration curve of the liquid crystal sheet relating the substrate temperature to the hue scale. (b) The picture shows the RGB images obtained during the calibration step. These are further processed to get the HIS images. (Figure appears in color online).

Experimental Procedure

The condensing chamber is assembled with a small quantity of liquid inventory kept in the annular space at the lower portion of the apparatus. The chamber is then evacuated by a turbo-mechanical combo vacuum pump. A fraction of water flashes to vapor that fills up the chamber. The evacuation process is continued for several minutes to ensure complete removal of noncondensable gases in the chamber. At this stage it is ensured that the absolute pressure in the chamber is equal to the saturation pressure of the working fluid at the chamber temperature. Any operating temperature-pressure of the working fluid can be obtained by a suitable combination of coolant water temperature (flowing in the upper rectangular passage) and the heat input to the chamber by the circular heaters placed below.

Condensation in the form of pendant drops commences almost immediately after evacuation is initiated. Hence, it is not possible to capture the liquid crystal thermographs in the initial phase of nucleation and droplet growth. Nucleated drops grow in size by direct condensation of the vapor and then by coalescence with the neighboring drops. Once the weight of the drop exceeds a certain threshold value, it falls back into the reservoir. An open virgin space is created at this location where fresh condensation is initiated. Thus, after the passage of a few minutes, a dynamic steady state of evaporation and condensation is established in the apparatus. The relevant data, namely, LCT images and condensations patterns of drops, have been acquired in the present work after quasi-steady-state is reached wherein growth of drops is primarily dominated by coalescence.

Data Reduction

The overall data reduction scheme applied to LCT images and condensation patterns at dynamic steady state is shown in Figure 3. Part (a) highlights the physical model considering a single condensing drop on the substrate. At a given instant of time, View A provides the actual photograph of drops distributed over the surface of the substrate, as recorded by the digital camera. The number density of drops as a function of diameter can be obtained from these data. View B is the corresponding liquid crystal thermograph of the substrate, as recorded by the color CCD camera. The instantaneous spatial distribution of temperature on the substrate is known via the TLC calibration curve. The color-to-temperature conversion scheme is explained in Figure 3b. It shows the actual image (View A), RGB image (View B), corresponding distribution of hue (and therefore the corresponding temperature, from Figure 2), and hue contours (temperature contours) over a selected area of the substrate, viz. region of interest. Individual condensing droplets and their corresponding base temperature distributions during condensation are clearly brought out with this approach.

For a given thermograph and its complementary photograph of the condensation pattern, heat transfer calculations can be carried out at the scale of a drop as well as the scale of the area imaged by the camera. The data reduction scheme adopted in this work for the two scales is as follows:

- Substrate level:

(a) Calculate the net heat flux from the entire substrate to the cooling water supply by assuming a one-dimensional heat transfer approximation.

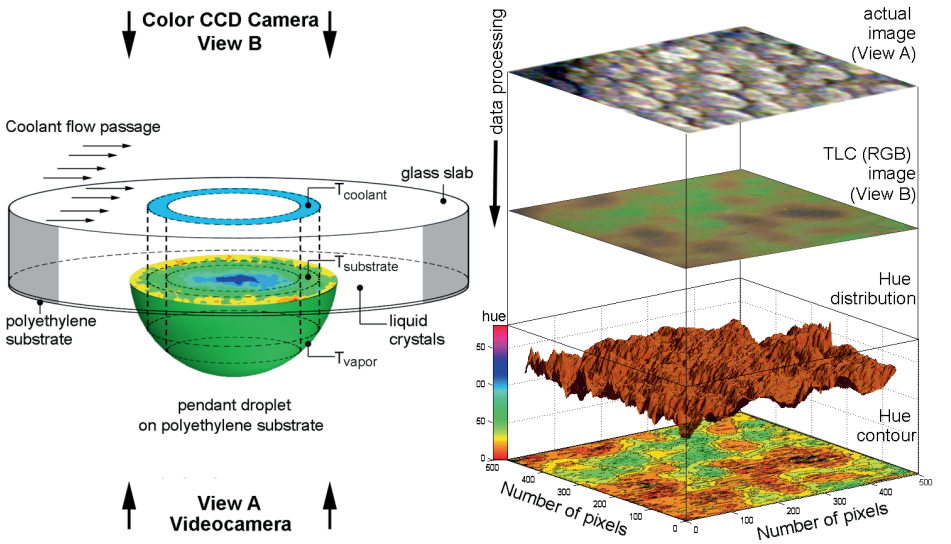

Figure 3. (a) The schematic shows the overall scheme for the estimation of the local heat transfer coefficient for drop-wise condensation occurring on the underside of the substrate. View A provides the direct picture of the drop, whereas View B provides the liquid crystal thermograph. (b) The figures shows the series of operations employed for data reduction. The image of condensing droplets is obtained from Camera View A, and the corresponding TLC RGB image is simultaneously obtained from Camera View B. The latter image provides the spatial hue distribution on the selected portion of the substrate, the contours of which can be transformed into spatial temperature distribution from the hue-temperature calibration curve. (Figure appears in color online).

(b) Calculate the heat transfer coefficient during drop-wise condensation by the net heat transfer rate obtained in step (a) and dividing it by the applicable degree of subcooling $(\bar{T}_{vap} - \bar{T}_{sub})$, where $\bar{T}_{sub}$ is the space-averaged temperature on the polymer substrate, as estimated from the liquid crystal thermograph.

Thus, considering one-dimensional heat transfer through the entire system, the instantaneous local heat flux through a unit pixelized area on the substrate is calculated as:

$$q''_{pix} = (\dot{Q}_{pix}/A_{pix}) = k_{glass} \cdot (T_{pix} - T_w)/t_{glass} \tag{1}$$

The net heat transfer from the individual droplet and the entire substrate, respectively, to the cooling water can be estimated as:

$$\dot{Q}_{drop}\big|_{exp} = \oint_{drop\ base\ area} q''_{pix} dA_{pix} \tag{2}$$

$$\dot{Q}_{total}\big|_{exp} = \oint_{total\ substrate\ area} q''_{pix} dA_{pix} \tag{3}$$

The average temperatures of the base area of individual pendant drops and the complete condensing substrate (in the experiments, $A_{sub} = A_{glass}$) are estimated respectively by area averaging the local pixel temperatures on the substrate, as follows:

$$\bar{T}_{sub} = \left(\frac{1}{A}\right) \oint_{total\ substrate\ area} T_{pix} \cdot dA_{pix} \tag{4}$$

$$\bar{T}_{drop} = \left(\frac{1}{A}\right) \oint_{drop\ base\ area} T_{pix} \cdot dA_{pix} \tag{5}$$

The average condensation heat transfer during drop-wise condensation is a direct manifestation of the combination of interfacial resistance to condensation of vapor on the drop surface and the diffusional resistance the droplet offers. Knowing the mean condensing vapor temperature inside the chamber, the steady-state average drop-wise condensation heat transfer through the polymer substrate can be estimated as:

$$\bar{h}_{\exp} = \left(\frac{\dot{Q}_{total}\big|_{\exp}}{A_{sub}(\bar{T}_{vap} - \bar{T}_{sub})}\right) \tag{6}$$

- Droplet level:

(a) Isolate individual droplets on the substrate; i.e., through respective complementary images of Views A and B.
(b) Calculate heat transfer rate from the base area of the individual droplet to the coolant and compare it with the one-dimensional heat throughput for an individual droplet. The latter accounts for interfacial heat transfer resistance, diffusion resistance through the droplet, and constriction resistance due to droplet curvature. The droplet geometry is assumed to be hemispherical, as confirmed with static contact angle measurements of pendant droplets on the surface. Dynamic contact angles could not be measured with this setup.

A one-dimensional model that takes into account heat transfer through individual droplet has been described by many authors (e.g., see Carey [12] and Graham and Griffith [13]). Considering interfacial resistance, drop curvature resistance, and diffusional resistance, the average heat transfer through the base of the droplet is given by:

$$(\bar{T}_{vap} - \bar{T}_{drop}) = \frac{2\dot{Q}_{drop}\big|_{model}}{h_i \cdot \pi \cdot D_{drop}^2} + \frac{(\bar{T}_{vap} - \bar{T}_{drop})D_{\min}}{D_{drop}} + \frac{\dot{Q}_{drop}\big|_{model}}{2k_{liq} \cdot \pi \cdot D_{drop}} \tag{7}$$

where the interface heat transfer coefficient h_i is given by:

$$h_i = \left(\frac{2\hat{\sigma}}{2 - \hat{\sigma}}\right) \frac{h_{fg}^2}{\bar{T}_{vap}\upsilon_{liq}} \left(\frac{M}{2\pi\tilde{R}T_{vap}}\right)^{0.5} \tag{8}$$

Thus, we can compare Eqs. (2) and (7) to validate the modeled and experimentally observed heat throughput across an individual droplet. In fact, if the complete range of droplet distribution is also estimated by the experiments then the total heat throughput from the substrate can be modeled as:

$$\dot{Q}_{total}\big|_{model} = \left(\frac{\pi \cdot (\bar{T}_{vap} - \bar{T}_{sub})}{2}\right) \int_{D_{min}}^{D_{max}} n_D \cdot D^2 \cdot \frac{(1 - D_{min}/D)}{(1/h_i + D/4k_l)} \cdot dD \tag{9}$$

Equation (9) can be compared with experimental estimation of the total heat throughput; i.e., Eq. (3). In the present experiments, due to limitations in optics, the smallest droplet that we could digitally measure with 99% confidence level was of the order of 0.4 mm. It is much larger than the minimum diameter of the drops that can possibly grow for a given wall subcooling [12]; namely,

$$D_{min} = \left(\frac{4 \cdot \upsilon_{liq} \cdot \sigma \cdot T_{sub}}{h_{fg}(T_{sat} - T_{sub})}\right) \tag{10}$$

Equation (10) yields $D_{\min}$ of the order of 0.01 mm. Hence, a large fraction of small drops could not be imaged in the present work. Because a large portion of the total heat flux is carried by droplets of small diameters, the verification of Eq. (9) with respect to Eq. (3) could not be conducted. This nonavailability of the droplet distribution function, especially in the lower droplet size range, is indeed a generic problem in experimental investigations of drop-wise condensation [1–3]. A practice that circumvents this difficulty is to assume a suitable distribution function of the small-sized drop in such a manner that it fits the experimental heat throughput. In this article we restrict our attention to single droplets in the range of ~0.35 mm to $D_{\max}$. The maximum diameter is a direct manifestation of the ratio of surface tension to the gravitational body force; i.e., the Bond number defined as:

$$D_{max} = K_1 \left(\frac{\sigma}{g(\rho_{liq} - \rho_{vap})}\right)^{0.5} \tag{11}$$

For the present experiments, $D_{\max}$ was obtained to be 4.73 mm ± 0.02 mm, which gives $K_1 = 1.732$ in Eq. (11).

RESULTS AND DISCUSSION

Drop shapes, condensation patterns, and LCT images during condensation are reported in the following sections. Of interest is the comparison of heat transfer rates calculated from drop-wise condensation patterns over the polyethylene surface of the LCT sheet, with those obtained from the one-dimensional simulation of the condensation process.

Contact Angle Measurements

Contact angles of static pendant droplets of water on polyethylene substrate were measured by a goniometer. The sample images of drops are shown in Figure 4.

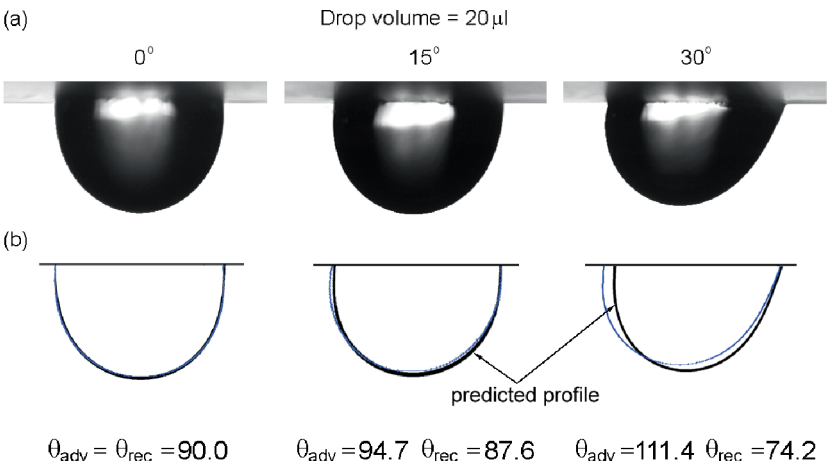

Figure 4. (a) Static contact angle of a pendant water droplet of 20 μL on a polyethylene substrate. The substrate is made to incline from the horizontal to study the effect of contact angle hysteresis. (b) Estimated droplet shapes generated with the assumption that the advancing front remains pinned are compared with the actual shape recorded in an experiment. (Figure appears in color online).

It can be clearly seen that there is considerable static contact angle hysteresis with increasing inclination of the substrate. The pendant drop shape can be conveniently estimated by a simple two-dimensional representation of the Young-Laplace equation; the numerical scheme for solving this equation is outlined in Appendix 1. Though the droplet contact line was assumed to be pinned in the calculations, this is not true for real surfaces. It can be seen that the droplet does not remain pinned to the surface as the inclination of the substrate is increased from the horizontal. For a horizontal substrate, the contact angles justify the use of a hemispherical geometry in the one-dimensional heat transfer model. However, it requires the assumption that dynamic contact angles realized during the time-dependent condensation process would be identical to those recorded under static conditions.

Heat Transfer through Individual Drops

Figure 5a shows the liquid crystal thermograph of a single droplet of diameter 2.96 mm condensing on the polyethylene substrate at a vapor saturation temperature of 41.1°C. In the LCT image, regions of high heat transfer rates appear as locations of relatively high temperature; for example, the blue ring in Figure 5a. Lower temperatures transit toward green and red. The hue distribution over the base of the droplet is shown in Figure 5b. Figure 5c shows the variation of heat throughput through the mid-plane passing through the single drop as identified in Figure 5a. Also shown in Figure 5d are examples of other isolated droplets recorded during the experiment. Figures 6a and 6b show a pair of adjacent droplets, condensing at vapor saturation temperature of 40.3°C, and the associated hue distribution on the base area. Figures 6c and 6d depict the instantaneous heat transfer rates through planes passing through these individual drops.

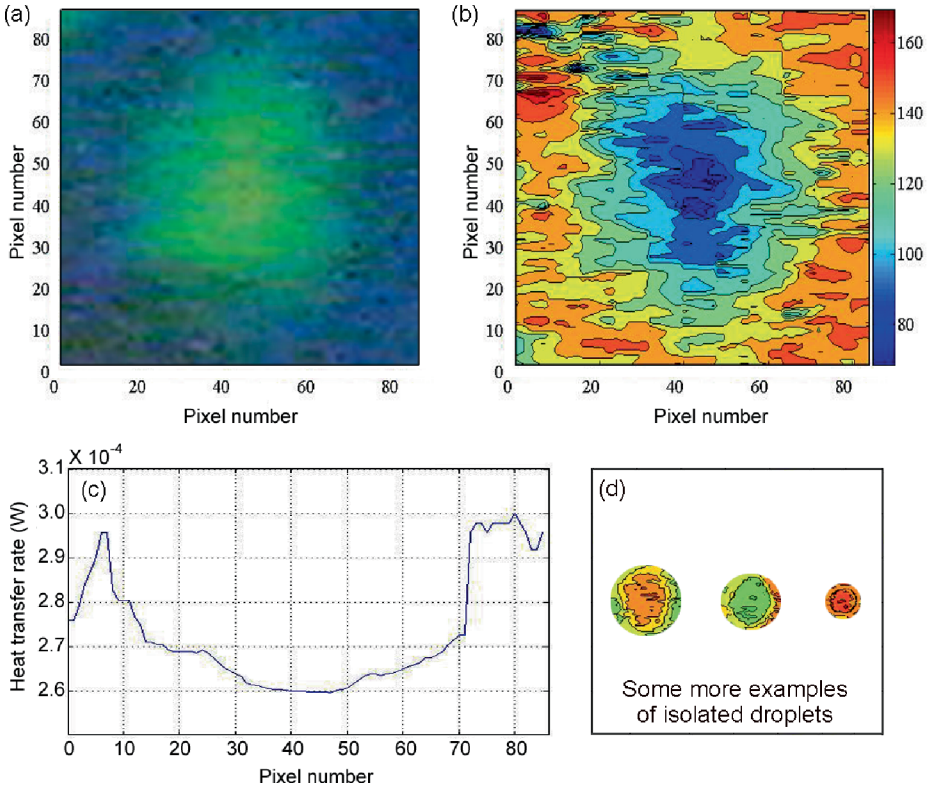

Figure 5. (a) and (b) The figures show the TLC-RGB image of an isolated pendant droplet (D = 2.96 mm) during drop-wise condensation process, at vapor saturation temperature of 40.3°C, and its corresponding hue contour plot. Images have been recorded after steady state has been attained. (c) The heat transfer rate at a plane passing through the middle of the droplet is shown as a function of position. (d) Examples of hue profiles of three other isolated droplets of smaller sizes. (Figure appears in color online).

Many interesting qualitative features can be noted from the data in Figures 5 and 6.

(a) Iso-hue lines (i.e., isotherms) can be clearly seen on the base area of the condensing pendant droplets. Thus, for a given temperature difference between the glass plate and the condensing vapor, the varying degree of droplet thermal resistance due to its changing thickness is clearly manifested as temperature distribution over the base of the drop.
(b) Maximum heat transfer rate appears near the apparent contact line of the pendant droplet. This is the zone where the thickness of the droplet is lowest, thus indicating the least thermal resistance.
(c) Immediately circumscribing the apparent contact line of the pendant drop there exists an adsorbed liquid thin film, which increases the thermal resistance to heat flow.
(d) The central portion of the drop poses the maximum heat transfer resistance.
(e) Smaller drops have a lower thermal resistance per unit area than larger drops.

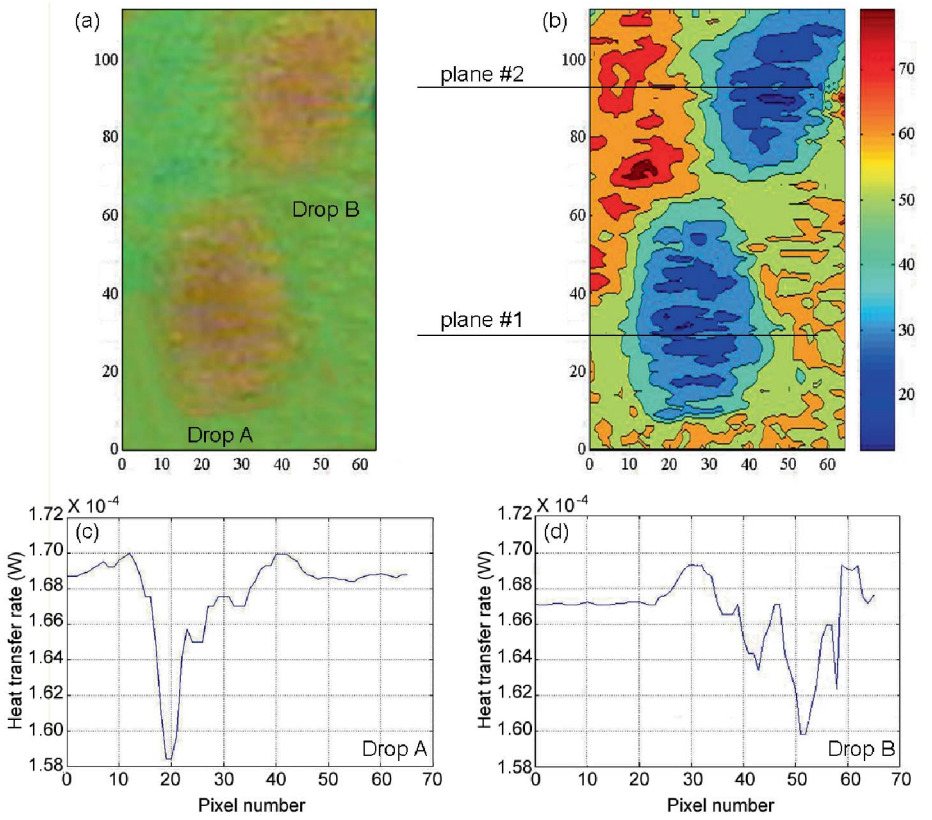

Figure 6. (a), (b) The figures show the TLC-RGB image of two adjacent pendant droplets during the dropwise condensation process and the corresponding hue contour plot at vapor saturation temperature of 40.3°C. Images have been acquired at steady state. (c), (d) Heat transfer rate through plane #1 (Drop A) and plane #2 (Drop B) is presented as a function of position. (Figure appears in color online).

The above observations are in agreement with the one-dimensional heat transfer model described previously.

Figure 7 shows the computed heat transfer rates through individual droplets as a function of drop diameter and degree of subcooling. Equations (7 through 9 have been used for the purpose. Following the literature [12, 24, 25], the accommodation coefficient for water has been taken to be unity. The computations have been performed at average vapor saturation temperature, $\bar{T}_{sat} = 41.0°C$.[1] The degree of subcooling $(\bar{T}_{vap} - \bar{T}_{sub})$ is varied from 0.4 to 2.0°C, as shown in Figure 7. Two bands of computed data are shown; one set corresponds to results obtained by neglecting the thermal resistance of the polyethylene substrate, whereas the other set corresponds to the case wherein this thermal resistance is included in the one-dimensional heat transfer model

[1]The change in thermophysical properties of water between the temperature range $39°C \leq \bar{T}_{sat} \leq 42°C$ is such that the heat flux estimate through the droplets is not substantially affected in this small range; the ensuing difference is minor and cannot be highlighted on a log-log scale used in Figure 7. Therefore, representative calculations have been shown at an average saturation temperature of 41.0°C.

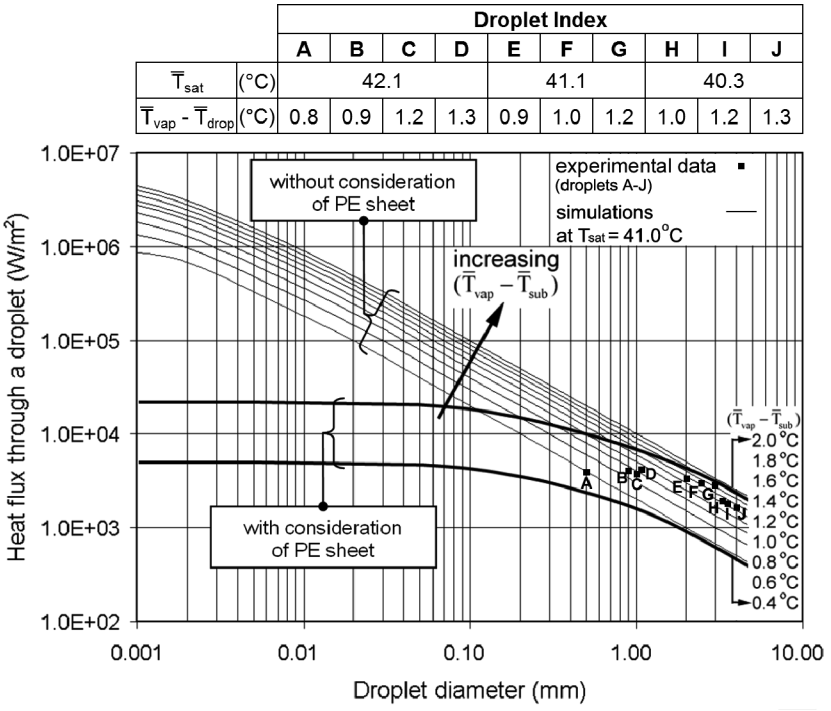

Figure 7. The figure shows heat flux variation over the base area of a drop as a function of the drop diameter. Experimental heat transfer rates through isolated droplets (A–J) have been determined from LCT data. The simulation at $T_{sat} = 41.0°C$ is (i) without and (ii) with the thickness of the PE substrate taken into account. Although the highest heat flux passes through the small drops, the thermal resistance due to small droplets diminishes with decreasing diameter (see Figure 8), and the resistance due to the PE foil starts dominating, thereby hindering heat transfer through the smaller diameter droplets.

(represented by thick set of lines). When the thermal resistance due to the polyethylene sheet is not considered, heat flux passing through the droplets drastically increases with decreasing droplet diameter; i.e., the maximum heat flux passes through the smallest diameter droplets. The inclusion of the thermal resistance due to the polyethylene sheet severely decreases the overall heat transfer, as shown in Figure 7. This deterioration effect is the most for smaller-sized droplets. Thus, for the present experiments, low thermal conductivity of the polyethylene sheet results in a large reduction in heat transfer through the smaller droplets.

The individual thermal resistances that constitute the overall thermal resistance are shown in Figure 8. It is clear from this figure that below a droplet diameter of about 0.5 mm, the thermal resistance due to the polyethylene sheet exceeds that of the diffusive resistance of the droplet. In addition, the interface heat transfer coefficient and the added thermal resistance due to the curvature of the droplet are not significant constituents in the overall thermal resistance. The curvature resistance becomes significant for extremely small droplets. For diameters beyond ~1.5 mm, the major resistance is due to the conduction within the droplet.

Figure 7 also shows the experimentally obtained heat flux through individual droplets. As stated previously, the minimum droplet diameter that could be measured

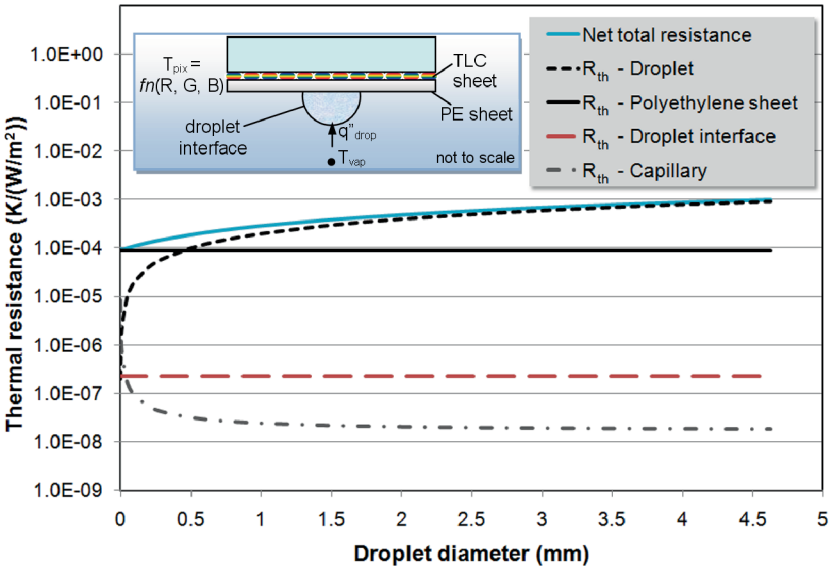

Figure 8. The variation of net thermal resistance of the substrate-droplet combined system (see inset) and its various components with the droplet diameter is shown. Below a droplet diameter of about 0.4 mm, the thermal resistance due to the PE sheet dominates the overall net resistance. Above a droplet diameter of 1.5 mm, droplet conductance is the dominating parameter. (Figure appears in color online).

in the present experiment was of the order of 0.4 mm, whereas the maximum droplet sizes were about 4.73 mm in diameter. In this range, Figure 7 shows data for 10 representative droplets isolated on the substrate; relevant details of these 10 droplets (indexed A through J) are also shown in Figure 7. As can be seen, deviation from the predicted values becomes greater as the droplet size; that is, the thermal resistance through the drop decreases. Data reduction for droplets below about 0.5 mm would not have resulted in meaningful conclusions because thermal resistance of the polyethylene sheet is dominant below this diameter. Moreover, for very small droplets, the temperature differences and geometrical length scales are too small to be resolved by the present technique as highlighted by Wang et al. [26]. Reasonable accuracy is obtained with the one-dimensional model of heat transfer for larger sized drops.

The average heat transfer coefficient estimated by using Eq. (6) is found to be sensitive to the extent of subcooling; namely, the vapor-to-substrate temperature difference. Specifically, for an increase in the average condensing vapor temperature, heat transfer coefficient increases from 4470 W/m^{2}K at 40.6°C to 5650 W/m^{2}K at 41.1 and 7580 W/m^{2}K at 42.1°C.

In this study we have focused our attention only on a horizontally placed substrate. It should be noted that, for an inclined substrate, the condensation pattern is dominated not only by coalescence of drops but also by the subsequent instability resulting in drop sliding/rolling motion down the inclined surface of the substrate. The sliding/rolling droplet wipes away portions of substrate area, subsequent to which fresh nucleation is initiated on the freshly wiped areas. This temporal wiping action of the unstable drops, superimposed on regularly condensing droplet patterns, leads to intricate local heat transfer mechanisms. The sliding/rolling droplet motion is also

affected by surface type and roughness, contact line dynamics, apparent contact angle hysteresis, etc. The ensuing phenomena is strongly time dependent; new timescales have to be addressed under such conditions.

CONCLUSIONS

The use of liquid crystal thermography for detecting the spatial temperature profile of individual condensing pendant droplets of pure water on a horizontally placed transparent polymer substrate has been attempted. Clear drop-wise condensation of water was achieved on this surface. Vivid isotherms on the condensing droplet base could be distinctly observed. Both normal light videography and liquid crystal thermography could be performed simultaneously in the uniquely designed test section. The local and average heat transfer coefficients on the substrate were estimated by data reduction and were found to be broadly comparable with the one-dimensional heat transfer approximation. The periphery of the droplet base line was seen to provide the path of least resistance for heat transfer. Average heat transfer rate increased with increase in subcooling and saturation pressures. The principal finding of the study is that it is adequate to image drop-wise condensation patterns on a surface. These images can be used to estimate local and average heat transfer coefficients by including the relevant thermal resistances between the condensing vapor and the subcooled substrate. Microscale measurement of small temperature differences continues to be a challenge for accurate estimation of heat transfer during drop-wise condensation. In this context, although liquid crystal thermography stretches the limit of spatial resolution to microscales, below this limit, temperature differentials are too small for correct and repeatable experimental determination and, therefore, application of numerical means becomes necessary.

REFERENCES

1. J.W. Rose, Dropwise Condensation Theory and Experiment: A Review, *Proceedings of the Institution of Mechanical Engineers*, vol. 216, pp. 115–128, 2002.
2. J.W. Rose, Condensation Heat Transfer Fundamentals, *Transactions of the IChemE*, vol. 76(A), pp. 143–152, 1998.
3. J.W. Rose, Dropwise Condensation Theory, *International Journal of Heat and Mass Transfer*, vol. 24, pp. 191–194, 1981.
4. A. Leipertz and A.P. Fröba, Improvements of Condensation Heat Transfer by Surface Modifications, *Proc. 18th National & 7th ISHMT-ASME Heat & Mass Transfer Conference*, Paper no. HMTC-2006-K7, pp. K85–K99, 2006.
5. S. Vemuri, K.J. Kim, B.D. Wood, S. Govindaraju, and T.W. Bell, Long Term Testing for Dropwise Condensation Using Self-Assembled Monolayer Coatings of n-Octadecylmercaptan, *Applied Thermal Engineering*, vol. 26, pp. 421–429, 2006.
6. A. Bani Kananeh, M.H. Rausch, A.P. Fröba, and A. Leipertz, Experimental Study of Dropwise Condensation on Plasma-Ion Implanted Stainless Steel Tubes, *International Journal of Heat and Mass Transfer*, vol. 49, pp. 5018–5026, 2006.
7. R.J. Goldstein, W.E. Ibele, S.V. Patankar, T.W. Simon, T.H. Kuehn, P.J. Strykowski, K.K. Tamma, J.V.R. Heberlein, J.H. Davidson, J. Bischof, F.A. Kulacki, U. Kortshagen, S. Garrick, and V. Srinivasan, Heat Transfer—A Review of 2003 Literature, *International Journal of Heat and Mass Transfer*, vol. 49, pp. 451–534, 2006.

8. X. Ma, J.W. Rose, D. Xu, J. Lin, and B. Wang, Advances in Dropwise Condensation Heat Transfer: Chinese Research, *Chemical Engineering Journal*, vol. 78, pp. 87–93, 2003.
9. J.A. Venables, *Introduction to Surface and Thin Film Processes*, Cambridge University Press, 2000.
10. J.W. Rose, Surface Tension Effects and Enhancement of Condensation Heat Transfer, *Chemical Engineering Research and Design*, vol. 82, pp. 419–429, 2004.
11. J.G. Collier, Convective Boiling and Condensation, 2nd ed., McGraw Hill, New York, 1981.
12. V.P. Carey, Liquid-Vapor Phase Change Phenomena, 2nd ed., Taylor and Francis, 2007.
13. C. Graham and P. Griffith, Drop Size Distributions and Heat Transfer in Dropwise Condensation, *International Journal of Heat and Mass Transfer*, vol. 16, pp. 337–346, 1973.
14. M. Abu-Orabi, Modeling of Heat Transfer in Dropwise Condensation, *International Journal of Heat and Mass Transfer*, vol. 41, pp. 81–87, 1998.
15. D. Beysens, Dew Nucleation and Growth, *Comptes Rendus Physique*, vol. 7, pp. 1082–1100, 2006.
16. B.J. Briscoe, D.R. Williams, and K.P. Galvin, Condensation on Hydrosol Modified Polyethylene, *Colloids and Surfaces A*, vol. 264, pp. 101–105, 2005.
17. X. Ma, J. Chen, D. Xu, J. Lin, C. Ren, and Z. Long, Influence of Processing Conditions of Polymer Film on Dropwise Condensation Heat Transfer, *International Journal of Heat and Mass Transfer*, vol. 45, pp. 3405–3411, 2002.
18. C.W.M. van der Geld, F.L.A. Ganzevles, C.T.P.F. Simons, and F. Weitz, Geometry Adaptations to Improve the Performance of Compact Polymer Condensers, *Transactions of the IChemE*, vol. 79(A), pp. 357–362, 2001.
19. *Handbook of Thermochromic Liquid Crystal Technology*, Hallcrest Publication, 2008. Available at http://www.hallcrest.com/downloads/randtk_TLC_Handbook.pdf (accessed October 14, 2008).
20. J. Stasiek, A. Stasiek, M. Jewartowski, and M.W. Collins, Liquid Crystal Thermography and True-Color Digital Image Processing, *Optics & Laser Technology*, vol. 38, pp. 243–256, 2006.
21. R. Muwanga and I. Hassan, Local Heat Transfer Measurements in Microchannels Using Liquid Crystal Thermography: Methodology Development and Validation, *ASME Journal of Heat Transfer*, vol. 128, pp. 617–627, 2006.
22. J.L. Hay and D.K. Hollingsworth, Calibration of Micro-Encapsulated Liquid Crystals Using Hue Angle and a Dimensionless Temperature, *Experimental Thermal and Fluid Science*, vol. 18, pp. 251–257, 1998.
23. C. Höhmann and P. Stephan, Microscale Temperature Measurement at an Evaporating Liquid Meniscus, *Experimental Thermal and Fluid Science*, vol. 26, pp. 157–162, 2002.
24. F. Peters and K.A.J. Mayer, Measurement and Interpretation of Growth of Monodispersed Water Droplets Suspended in Pure Vapor, *International Journal of Heat and Mass Transfer*, vol. 38, pp. 3285–3293, 1995.
25. V.P. Carey and S.M. Oyumi, Condensation Growth of Single and Multiple Water Microdroplets in Supersaturated Steam: Molecular Simulation Predictions, *Microscale Thermophysical Engineering*, vol. 1, pp. 31–38, 1997.
26. Y.X. Wang, J.L. Plasky, and P.C. Wayner, Jr., Optical Measurement of Microscale Transport Processes in Dropwise Condensation, *Microscale Thermophysical Engineering*, vol. 5, pp. 5–55, 2001.

APPENDIX 1

The Young-Laplace equation

$$2\kappa_{\mathrm{m}} = \frac{\Delta\rho}{\sigma}\mathrm{g}\cdot\mathrm{y} + \mathrm{B} \tag{A1}$$

is solved in two dimensions with the mean curvature given by [8]:

$$\kappa_{\mathrm{m}} = -\frac{1}{2}\left(\frac{\mathrm{y}''}{\left(1+\mathrm{y}'^2\right)^{\frac{3}{2}}}\right) \tag{A2}$$

Here B is the excess pressure inside the drop. Thus, the governing equation for a pendant drop is

$$\frac{\mathrm{d}^2\mathrm{y}}{\mathrm{dx}^2} = -\left(1+\left(\frac{\mathrm{dy}}{\mathrm{dx}}\right)^2\right)^{\frac{3}{2}}\left(\frac{\mathrm{y}}{\mathrm{l}^2}+\mathrm{B}\right) \tag{A3}$$

with the boundary conditions at a starting point:

$$\begin{aligned} &\mathrm{y}(\mathrm{x}=0) = 0 \\ &\frac{\mathrm{dy}}{\mathrm{dx}}(\mathrm{x}=0) = -\tan\theta \end{aligned} \tag{A4}$$

Equations (A1)–(A4) can be generalized to stable pendant and sessile drops on inclined surfaces. Here the appropriate component of acceleration due to gravity is utilized, depending on the orientation of the drop. In addition, it should be noted that boundary conditions employing unequal advancing/receding angles would yield drop shapes that lack geommetrical symmetry.

The second-order ordinary differential equation with boundary conditions is solved along with the constraint of a given droplet volume using a fourth-order Runge-Kutta scheme. The solution of the governing equation yields the droplet profile. The model assumes that the drop is pinned at the line of contact. This may not always be true and the advancing point may move with substrate inclination.